AUTHOR(S)
Liu, X., Zhu, J., Zhang, Q., Hu, H., Zhang, W., Xu, H., Huang, Y., Xie, J., Liu, H., Feng, Y., Li, J., & Jia, C.

TITLE
Multifunctional fluorescent probe for simultaneous revealing Cys and ONOO– dynamic correlation in the ferroptosis

YEAR
2024

DOI
10.1016/j.saa.2024.124248

CITATION
Liu, X., Zhu, J., Zhang, Q., Hu, H., Zhang, W., Xu, H., Huang, Y., Xie, J., Liu, H., Feng, Y., Li, J., & Jia, C. (2024). Multifunctional fluorescent probe for simultaneous revealing Cys and ONOO– dynamic correlation in the ferroptosis. *Spectrochimica Acta Part A: Molecular and Biomolecular Spectroscopy, 315*, 124248. https://doi.org/10.1016/j.saa.2024.124248

VERSION
Accepted Manuscript

Multifunctional fluorescent probe for simultaneous revealing Cys and $ONOO^-$ dynamic correlation in the ferroptosis

Xiongbo Liu [a†], Jiali Zhu [a†], Qiangsheng Zhang [a d], Hao Hu [a], Wei Zhang [e], Hui Xu [f], Yan Huang [h], Jialin Xie [a d], Hongtao Liu [a d], Yan Feng [a d*], Jianwei Li [c*], Chunman Jia [a b d*]

[a]*Hainan Provincial Key Laboratory of Fine Chem, School of Chemistry and Chemical Engineering, Hainan University, Haikou 570228, China.*

[b]*Analysis and Testing Center, Hainan University, Haikou 570228, China.*

[c]*MediCity Research Laboratory, University of Turku, Tykistökatu 6, Turku, 20520, Finland*

[d]*One Health Institute, Hainan University, Haikou, 570228, China*

[e]*Key Laboratory of Hainan Trauma and Disaster Rescue, The First Affiliated Hospital of Hainan Medical University, Hainan Medical University, Haikou, 571199 P. R. China*

[f]*Institute for Energy Research, School of the Environment and Safety Engineering, Jiangsu University, Zhenjiang 212013, P.R. China*

[h]*School of Chemistry and Chemical Engineering, Jiangsu University, Jiangsu 212013, China*

[†] Xiongbo Liu and Jiali Zhu contributed equally to this work and should be regarded as co-first authors.

Abstract

Ferroptosis is a type of lipid peroxidation-induced apoptosis brought on by imbalances in iron metabolism and redox. It involves both the thiol-associated anti-ferroptosis pathway and the excessive buildup of reactive oxygen species (ROS), which stimulates the ferroptosis pathway. Determining the precise control mechanism of ferroptosis requires examining the dynamic connection between reactive sulfur species (RSS) and ROS. Cysteine (Cys) and peroxynitrite ($ONOO^-$) are highly active redox species in organisms and play dynamic roles in the ferroptosis process. In this study, a

* Corresponding author: E-mail address: fengy@hainanu.edu.cn
* Corresponding author: E-mail address: jianwei.li@utu.fi
* Corresponding author: E-mail address: jiachunman@hainanu.edu.cn

coumarin dye was conjugated with specific response sites for Cys and $ONOO^-$, enabling the simultaneous detection of Cys and $ONOO^-$ through the green and red fluorescence channels, respectively (λ_{em} = 498 nm for Cys and λ_{em} = 565 nm for $ONOO^-$). Using the probe **LXB**, we monitored the changes in Cys and $ONOO^-$ levels in the ferroptosis pathway induced by erastin. The results demonstrate a significant generation of $ONOO^-$ and a noticeable decrease in intracellular Cys levels at the beginning upon erastin treatment and finally maintains a relatively low level. This study presents the first probe to investigate the intracellular redox modulation and control between Cys and $ONOO^-$ during ferroptosis, providing valuable insights into the potential mutual correlation between Cys and $ONOO^-$ in this process.

Keywords: fluorescent probe; dual-channel; Cys and $ONOO^-$; ferroptosis

1. Introduction

Ferroptosis as a unique process of cell death, is a classic symptom of redox imbalance [1]. It also involves complex molecular mediation mechanisms, such as iron accumulation, lipid peroxidation, amino acid metabolism, system X_c^-, and glutathione peroxidase4 (GPX4) [2-4]. The regulatory mechanism of ferroptosis is also extremely complex, and its regulatory mechanism depends on ROS and RSS [5,6]. Among them, $ONOO^-$ can be endogenously produced by coupling superoxide anions (O_2^-) and nitric oxide (NO) radicals [7-9]. It has strong oxidizing properties and can participate in many pathological processes [10-12]. High concentrations of $ONOO^-$ and imbalanced iron metabolism can lead to lipid peroxidation, resulting in cellular iron toxicity, ultimately leading to ferroptosis [13]. Cys, as one of the most abundant and important biological thiols in living organisms, is also common in many physiological processes [14-16]. Cys serves as a precursor to glutathione (GSH), GSH can be produced through the cysteine/glutamate reverse transporter protein (system X_c^-) [17-20]. And GSH, by maintaining the reactivity of GPX4, can prevent lipid peroxidation and serve as a key regulatory factor for ferroptosis [21-24]. Thus, Cys has been applied as one of the important metabolites for detecting ferroptosis [25]. Nowadays, there are some common ferroptosis inducers on the market that disrupt the body's redox balance by

interfering with Cys levels or reactive $ONOO^-$, thereby promoting ferroptosis [26-29]. The conclusion can be drawn that Cys and $ONOO^-$ play critical and interconnected roles in the development and redox regulation of ferroptosis. Therefore, further investigation into the regulatory mechanisms and pathological functions of ferroptosis presents significant challenges. Moreover, developing an efficient method for detecting Cys and $ONOO^-$ in biological systems holds great significance.

Real-time visualization of Cys and $ONOO^-$ and the detection of their respective changes using a fluorescent probe is an efficient and convenient approach for exploring the modulation process [30-34]. While existing probes for Cys and $ONOO^-$ detection in ferroptosis have been reported [35-41], the use of a dual-functional probe would overcome the limitations of using two separate probes, such as potential spatiotemporal inhomogeneous distribution and cross-interference. Over the past few years, several fluorescent probes with dual response sites for ROS/RSS (GSH and H_2O_2, •OH and Cys, GSH and $ONOO^-$) have been developed for studying oxidative stress in ferroptosis [42-44]. However, the correlation between the involvement of Cys and $ONOO^-$ mechanisms in ferroptosis has not been reported.

In view of the aforementioned circumstances, a probe capable of visualizing redox processes in cells between Cys and $ONOO^-$ must fulfill three prerequisites: (1) The probe should exhibit distinct fluorescent responses towards Cys and $ONOO^-$; (2) The respective fluorescent responses should be independent of each other; (3) Sufficient sensitivity is required to detect endogenous levels. Considering these criteria, a coumarin-based dual-site probe **LXB** was designed to meet our needs (Scheme 1). This probe featured a selective Cys-reactive group that activated α, β-unsaturated double bonds, and an $ONOO^-$ reactive group that activated 4-bromomethyl phenylborate, resulting in a multifunctional probe. Upon response to Cys and $ONOO^-$, the green fluorescence increased and the red fluorescence quenched, leveraging distinct fluorescence channels (λ_{em}=498 nm, λ_{ex}=445 nm for Cys; λ_{em}=565 nm, λ_{ex}=470 nm for $ONOO^-$) to selectively visualize Cys and $ONOO^-$. Furthermore, cell imaging experiments demonstrated the effective application of **LXB** as a bioimaging chemosensor for exploring the mutual correlation between Cys and $ONOO^-$ in

ferroptosis. With the assistance of **LXB**, we revealed the flux of $ONOO^-$ and a decrease in Cys simultaneously during erastin-induced ferroptosis and eventually maintained at a relatively low level.

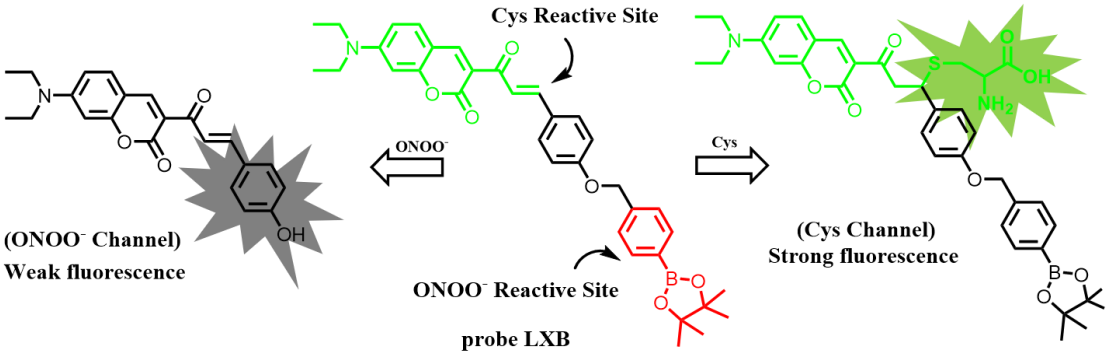

Scheme 1. Design principle of probe **LXB**.

2. Experimental section

2.1 Synthesis

Scheme 2 outlines the synthesis process for the probe **LXB**, which has been verified by ^1H NMR, ^{13}C NMR, and HRMS (Figures S1-S7). Compound **1** and compound **2** was synthesized according to the reported literature [45-46].

K_2CO_3 (242 mg, 1.66 mmol) was added to a stirred solution of compound **2** (300 mg, 0.82 mmol) and 4-bromomethylphenylboronic acid pinacol ester (490 mg, 1.66 mmol) in acetone (20 mL). The resulting solution was refluxed at 60℃ for 5 h in the sealed pressure vessel. TLC plate was used to track the reaction. Following the sample's cooling to ambient temperature and solvent removal under reduced pressure, the sample was purified using a silica gel flash column with an eluent mixture of petroleum ether and ethyl acetate (30:1-10:1, /v /v) to get probe **LXB** as an orange solid (261 mg, yield 55%). ^1H NMR (400 MHz, DMSO-d_6) δ 8.58 (s, 1H), 7.85 (d, J = 15.8 Hz, 1H), 7.72 – 7.63 (m, 6H), 7.47 (d, J = 8.0 Hz, 2H), 7.09 (d, J = 8.8 Hz, 2H), 6.81 (d, J = 6.6 Hz, 1H), 6.61 (d, J = 2.3 Hz, 1H), 5.22 (s, 2H), 3.50 (q, J = 7.0 Hz, 4H), 1.30 (s, 12H), 1.20 – 1.14 (m, 6H). ^{13}C NMR (101 MHz, DMSO-d_6) δ 185.86, 160.60, 160.41, 158.63, 153.38, 148.72, 142.38, 140.56, 135.06, 132.76, 130.71, 128.22, 127.34, 123.21, 116.15, 115.87, 110.64, 108.35, 96.35, 84.16, 69.61, 44.92, 25.14, 12.83. HRMS（ESI） m/z for $([C_{35}H_{38}BNO_6]+H)^+$: calcd: 580.2871, $([C_{35}H_{38}BNO_6]+H)^+$ found: 580.2864.

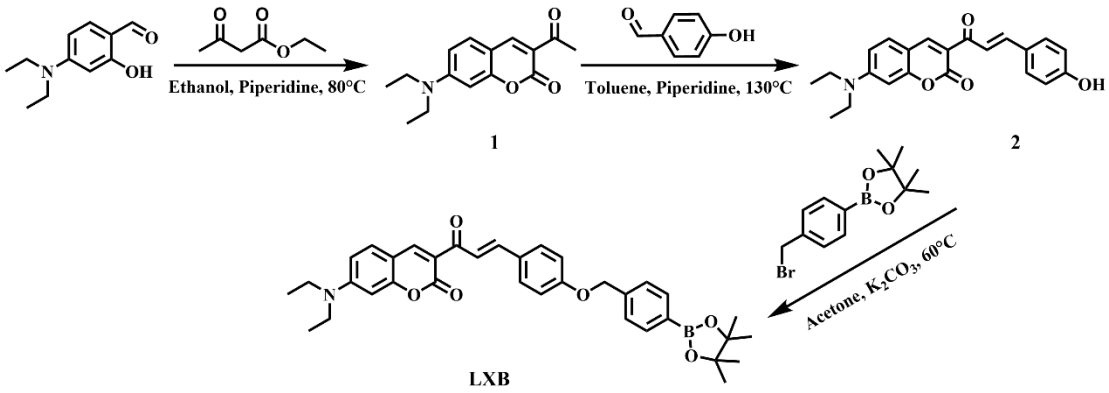

Scheme 2. Probe **LXB** synthetic route.

2.2. Theoretical calculations

All the simulation calculations were carried out with Gaussian 16 program package. The geometry optimization and electronic structure natures of probe and product at the level of B3LYP-GD3(BJ)/6-311G** have been evaluated. The implicit solvent model SMD was used, with water as the solvent. Time-dependent density functional theory (TD-DFT) calculations were performed based on the optimized molecular structure at the B3LYP-GD3(BJ)/6-311G** level [47].

2.3. Cell fluorescence imaging

HepG2 cells and **LXB** (10 μM) were co-incubated for 30 min. The fluorescence images were obtained on a confocal laser scanning microscope (OLYMPUS FV3000). λ_{ex}= 405 nm, λ_{em}= 460-500 nm (green channel), λ_{ex}= 488 nm, λ_{em}= 560-660 nm (red channel).

2.4. Ferroptosis imaging experiment

HepG2 cells were treated with 10 μM probe **LXB** for 30 min, ang then treated with 10 μM erastin or 10 μM erastin and 15 μM Fer-1 for various times (0-2 h).

3. Results and discussion

3.1. Design of probe

The probe **LXB** comprises a coumarin fluorophore as the fluorescence reporter, along with a selective Cys-reactive group that activates α, β-unsaturated double bonds, and an $ONOO^-$ reactive group that activates 4-bromomethyl phenylborate. Initially, **LXB** exhibits red fluorescence due to modifications of the coumarin dyes and an increase in conjugation. Upon reacting with Cys, a corresponding intermediate

thioether rapidly forms by the addition of the sulfhydryl functionality of Cys as the nucleophile to the α, β-unsaturated carbonyl moiety. This process releases a new fluorescent dye with strong green fluorescence, exhibiting a blue shift in fluorescence. 4-bromomethyl phenylborate is chosen as the response site for $ONOO^-$ due to its rapid reaction rate under mild conditions, as well as its highly selective recognition for $ONOO^-$ [48-50]. Upon reacting with $ONOO^-$, the activated 4-bromomethyl phenylborate is subsequently oxidized. This oxidation, coupled with the stronger electron withdrawing ability of -OH, leads to the formation of a strong "push-pull" system in the excited state via the ICT effect. Consequently, the absorption wavelength experiences a red shift, and the fluorescence is quenched.

3.2. Mechanism

The mechanism of detecting Cys and $ONOO^-$ using probe **LXB** was then investigated through HRMS assay, high-performance liquid chromatography (HPLC) and density functional theory (DFT) calculations. The HRMS data of the reaction product of **LXB** with Cys and $ONOO^-$ clearly showed a peak at 701.3040, corresponding to **LXB-Cys** (HRMS, calculated for $[M+H]^+$ 701.3069), and a peak at 386.1405, corresponding to compound **2** (HRMS, calculated for $[M+Na]^+$ 386.1465) (Figure 1A). Besides, we utilized a triple quadrupole liquid chromatograph mass spectrometer for analyzing the reaction process and final products. The mobile phase of the reversed-phase column employed in the experiment consisted of CH_3CN: H_2O (4:1, v/v) (Figure S8A). The HPLC chromatogram illustrates a retention time of 9.10 min for **LXB**, corroborated by the appearance of the 580.2 peak attributed to probe **LXB** $(M+H)^+$ in the HRMS diagram (Figure S8B). Upon addition of Cys to the probe **LXB**, the peak intensity of the probe diminished at 9.11 min, giving rise to a new peak at 1.48 min, with the appearance of the 723.2 peak attributed to **LXB**-Cys $(M+Na)^+$. Furthermore, upon addition of $ONOO^-$ to the probe **LXB**, the 9.10 min peak vanished, replaced by a new peak at 1.45 min, accompanied by the appearance of the 364.1 peak attributed to **LXB**-$ONOO^-$ $(M+H)^+$ in the HRMS diagram (Figure S8C). These results align with our hypothesized mechanism, confirming its validity.

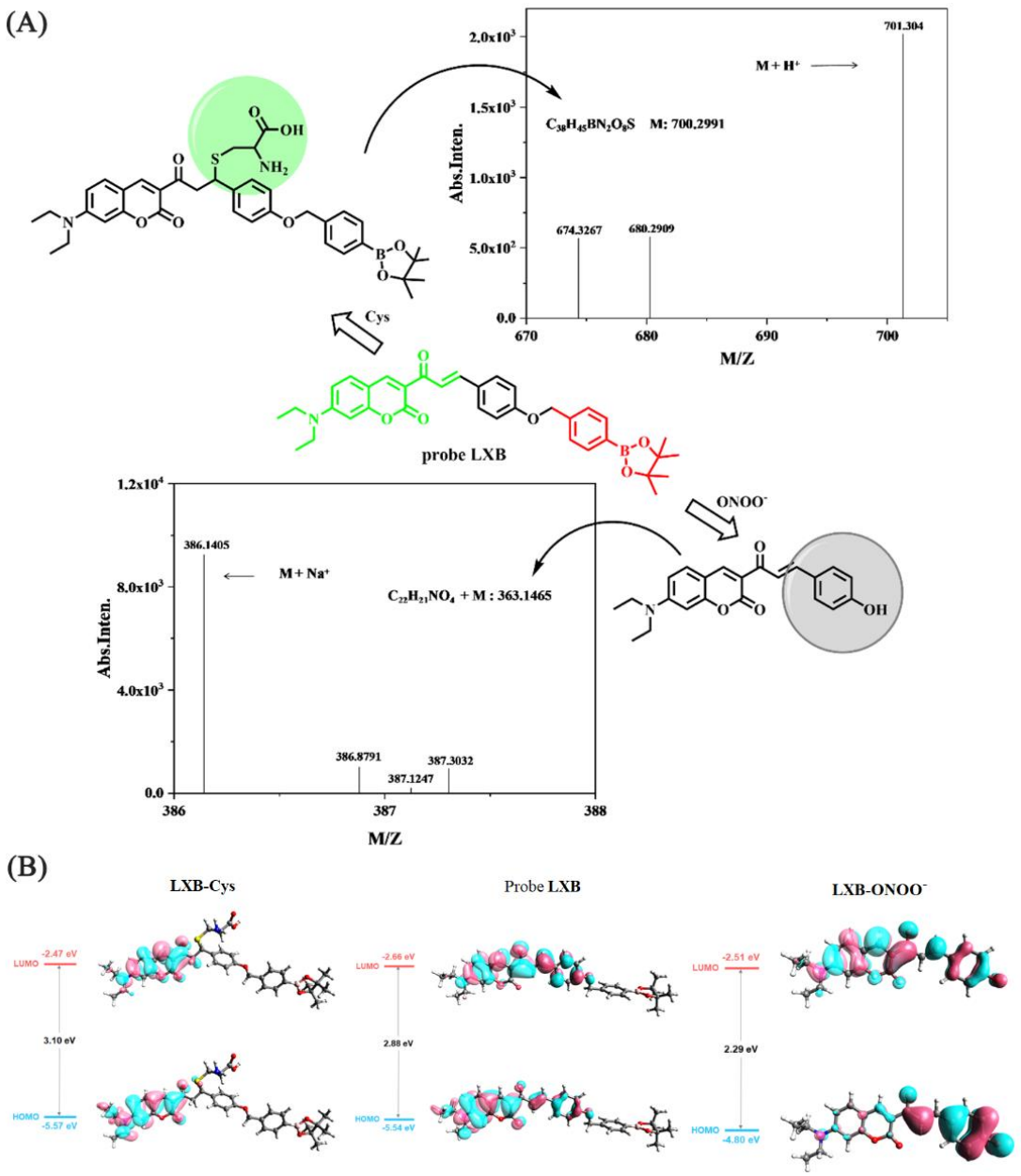

Figure 1. (A) HRMS data of **LXB**-Cys and **LXB**-ONOO$^-$; (B) TD-DFT calculation result of **LXB-Cys, LXB** and **LXB-ONOO**$^-$: energy gap, HOMO, and LUMO.

Furthermore, the electrons of probe **LXB** were found to be delocalized across the coumarin molecular skeleton on both the lowest unoccupied molecular orbital (LUMO) and the highest occupied molecular orbital (HOMO). In the presence of Cys, the conjugate structure of the probe changed, resulting in stronger fluorescence. This was because the energy gaps of **LXB-Cys** (3.10 eV) were larger than those of **LXB** (2.88 eV). On the other hand, the frontier molecular orbital map revealed that probe **LXB-ONOO**$^-$ had a delocalized electron cloud, with the electron distribution shifting from

the HOMO of the -OH group to the LUMO of the N-ethyl-N-methylethanamine group after excitation. This indicated strong migration of intramolecular charge transfer properties (ICT), leading to fluorescence quenching. The energy gaps of **LXB- ONOO$^-$** (2.29 eV) were lower than those of **LXB** (2.88 eV). This was consistent with the blue shift observed in the UV-vis spectra of **LXB** treated with Cys and the red shift observed in **LXB** treated with ONOO$^-$ (Figure 1B). Additionally, time-dependent density functional theory (TD-DFT) calculations were performed. The results, based on the optimized structure, showed that the absorbance maximum of **LXB** (470 nm), **LXB-Cys** (465 nm), and **LXB-ONOO$^-$** (505 nm) matched relatively well with the calculation results of **LXB** (457 nm, f = 1.46), **LXB-Cys** (402 nm, f = 0.39), and **LXB-ONOO$^-$** (524 nm, f = 1.02) (Figures S9-S11).

3.3 UV-vis and fluorescence spectra experiments

Initially, we conducted tests to determine the ability of the probe **LXB** to detect Cys and ONOO$^-$ in a solution of DMF/H_2O (4/6, v/v). When **LXB** (10 μM) was used without any other substances, it exhibited a weak absorption peak at 350 nm and a strong absorption peak at 470 nm (Figure 2A). As the concentration of Cys (0-60 equiv) increased, the absorption peaks gradually decreased, and a slight blueshift from 470 to 465 nm was observed. Additionally, the addition of ONOO$^-$ (0-10 equiv) resulted in a gradual decrease of the strong absorption peak at 470 nm and the emergence of a new peak at 505 nm, indicating a change in the molecular structure from **LXB** to compound **2** after ONOO$^-$ (Figure 2B).

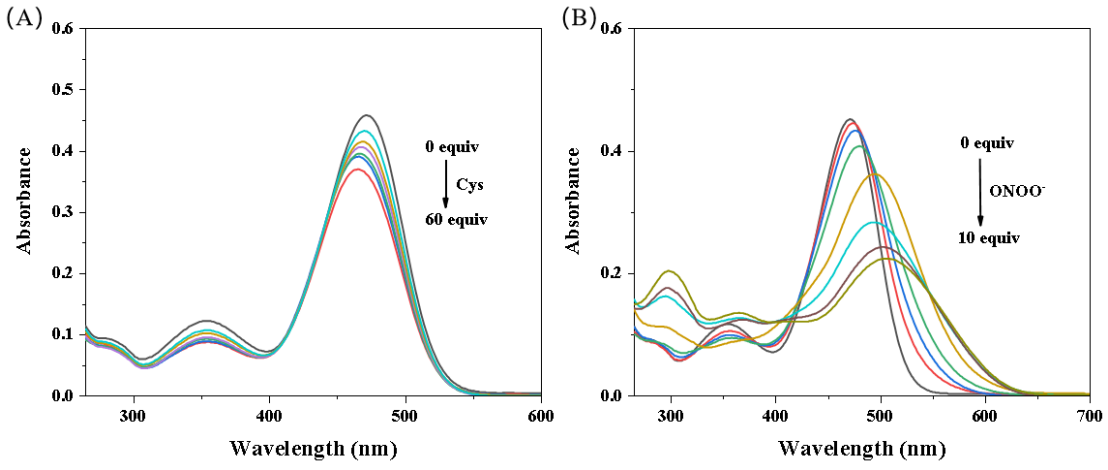

Figure 2. (A) as Cys (0-60 equiv) increases probe **LXB (**10 μM**)** changes in the UV-vis

absorption spectra. (B) as $ONOO^-$ (0-10 equiv) increases; probe **LXB** (10 μM) changes in the UV-vis absorption spectra. In DMF: H_2O (4/6, v/v).

Furthermore, by including varying concentrations of Cys (0-60 equiv) in the probe solution and exciting it at 445 nm, we observed a gradual enhancement of fluorescence at 498 nm and a gradual decrease in fluorescence intensity at 565nm. The isoemissive point was found to be 544 nm (Figure 3A). There was a clear linear relationship between the fluorescence intensity ratio ($F_{498\ nm}/F_{565\ nm}$) and the concentration of Cys (Figure 3C) with a strong correlation ($R^2 = 0.9968$). Using the formula DL=3 σ/k, we calculated the detection limit to be 1.31 μM.

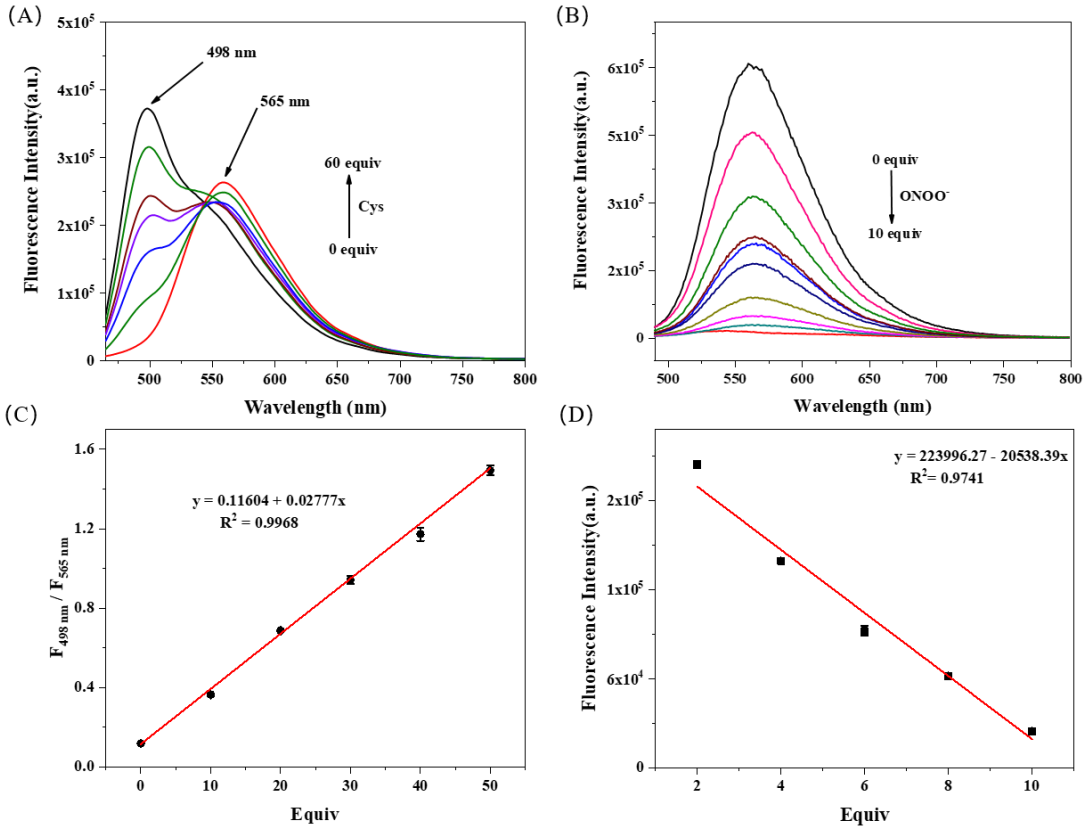

Figure 3. These are the fluorescence spectra of the following: (A) probe (10 μM) and Cys (0-60 equiv); (B) probe (10 μM) and $ONOO^-$ (0-10 equiv); (C) fluorescence intensity ratio ($F_{498\ nm}/F_{565\ nm}$) and the concentration of Cys (0-60 equiv); (D) probe (10 μM) and $ONOO^-$ (0-10 equiv) at 565 nm. Cys channel：λ_{ex} = 445nm，λ_{em} = 498 nm，slit = 2/2 nm. $ONOO^-$ channel：λ_{ex} = 470 nm，λ_{em} = 565 nm，slit = 2/2 nm.

Similarly, when we included varying concentrations of $ONOO^-$ (0-10 equiv) in the probe solution and excited it at 470 nm, we observed a gradual quenching of

fluorescence at 565 nm (Figure 3 B). Again, there was a linear relationship between the emission intensity and the concentration of $ONOO^-$ at a wavelength of 565 nm (Figure 3D) with a strong correlation (R^2 = 0.9741) (Figure 3D), and the detection limit was calculated to be 3.89 μM. These results indicate that **LXB** can effectively detect Cys and $ONOO^-$ with high sensitivity through different excitation and emission channels. Next, we systematically analyzed the reaction time spectra of **LXB** with Cys and $ONOO^-$. Under 445 nm excitation, the fluorescence intensity gradually increased at 498 nm upon introducing Cys (60 equiv) to **LXB** (10 μM) and eventually reached a plateau after 25 min (Figure S12A). Similarly, when excited at 470 nm, the probe exhibited intense fluorescence at 565 nm. Upon introducing $ONOO^-$ (10 equiv) to **LXB** (10 μM), the fluorescence intensity gradually decreased at 565 nm and eventually reached a plateau after 10 min (Figure S12B). These results indicate that **LXB** can rapidly detect Cys and $ONOO^-$ through different emission channels (λ_{em}=498 nm, λ_{ex}=445 nm for Cys; λ_{em}=565 nm, λ_{ex}=470 nm for $ONOO^-$).

3.4 Selective and interfering experiments

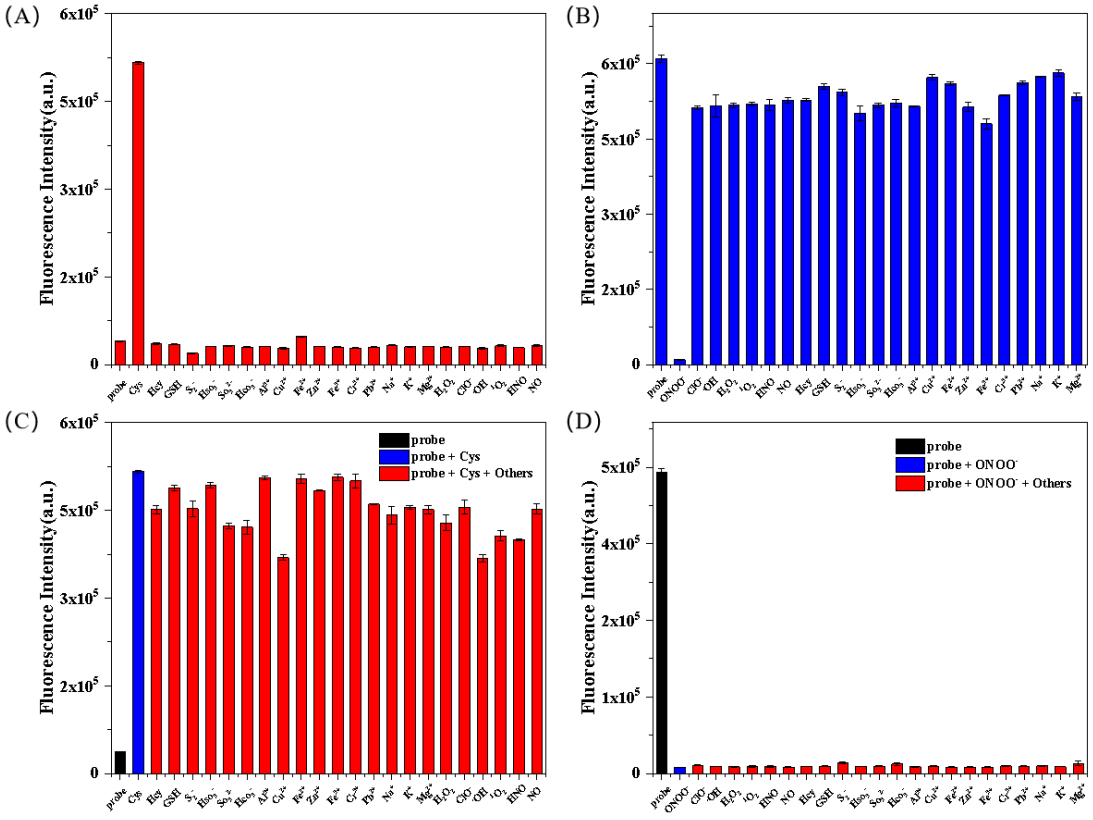

Figure 4. Selectivity and anti-interference fluorescence spectra of probes. (4A, 4C)

Probe **LXB** (10 μM) and Cys (60 equiv) and others ions (60 equiv) and S^{2-} (20 equiv); (4B, 4D) Probe **LXB** (10 μM) and $ONOO^-$ (10 equiv) and others ions (10 equiv). Other detecting substance: Na^+, K^+, Al^{3+}, Cu^{2+}, Fe^{2+}, Zn^{2+}, Fe^{3+}, Cr^{3+}, Pb^{2+}, Mg^{2+}, Hcy, GSH, HSO_3^-, S^{2-}, HCO_3^-, SO_3^{2-}, ClO^-, $^1O_2$, H_2O_2, ·OH, HNO, NO.

We performed experiments on Cys and $ONOO^-$ using different ions (Na^+, K^+, Al^{3+}, Cu^{2+}, Fe^{2+}, Zn^{2+}, Fe^{3+}, Cr^{3+}, Pb^{2+}, Mg^{2+}, Hcy, GSH, S^{2-}, HSO_3^-, HCO_3^-, SO_3^{2-}, ClO^-, $^1O_2$, H_2O_2, ·OH, HNO, NO) to further investigate the selective recognition and anti-interference capabilities of the probe **LXB**. The addition of other ions to **LXB** at 498 nm has no effect on the fluorescence intensity of Cys at 498 nm (Figure 4A, 4C). Meanwhile, it reveals that adding $ONOO^-$ and other ions to probe does not affect the fluorescence intensity of $ONOO^-$ at 565 nm (Figure 4B, 4D). It indicates that the probe has high selectivity and anti-interference ability towards Cys and $ONOO^-$ in different emission channels.

3.5 The influence of pH and MTT

Considering the crucial role of pH in the cellular microenvironment, we also examined the impact of the probe on Cys and $ONOO^-$ under varying pH conditions. We tested the fluorescence intensity of **LXB** (10 μM) at different pH values. As depicted in Figure 5A, the addition of Cys (60 equiv) to **LXB** (10 μM) resulted in an increase in fluorescence intensity at 498 nm within the pH range of 6-8. In contrast, the fluorescence intensity of the probe (10 μM) at 565 nm decreased at pH 6-8 after adding $ONOO^-$ (10 equiv), as illustrated in Figure 5B. Since the physiological pH level in the human body is weakly alkaline, we can conclude that **LXB** performs well in detecting Cys and $ONOO^-$ under normal physiological conditions. Furthermore, we tested the cell compatibility and toxicity of the probe. The results showed that the probe exhibited no significant cytotoxicity, indicating its suitability for live cell bioimaging (Figure S13).

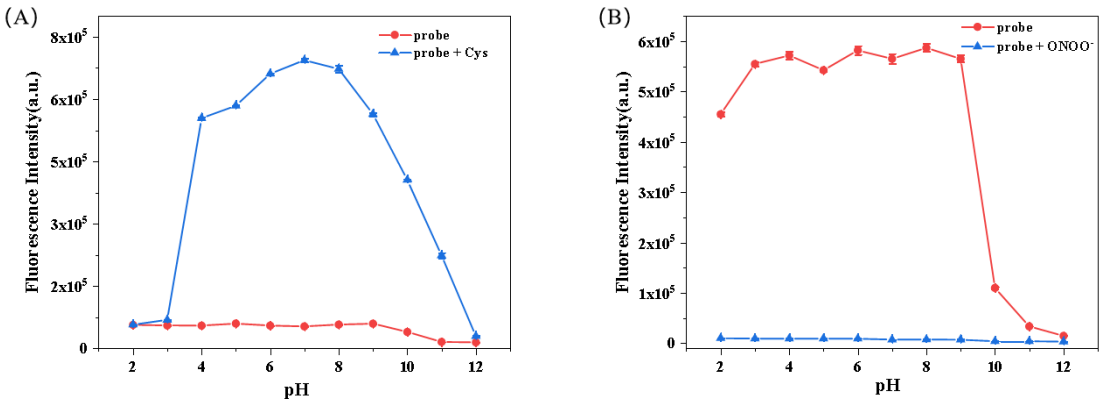

Figure 5. (A) The fluorescence intensity of probe **LXB** (10 μM) with and without and Cys (60 equiv); (B) The fluorescence intensity of probe **LXB** (10 μM) with and without and $ONOO^-$ (10 equiv). Solvent system: DMF/H_2O (10 mM,4:6, v/v) at different pH (2-12).

3.6 Fluorescent imaging in live cells

We then performed live cell bioimaging experiments on the probe using confocal microscopy. After treating HepG2 cells with probe **LXB (**10 μM**)** for 30 min, fluorescence was observed in both the green and red channels (Figure 6A). In addition, cells were pretreated with 2mM N-ethylmaleimide (NEM, a biological thiol detergent) for 1 h, followed by coincubation with probe **LXB** (10 μM) for 30 min. The result showed that the fluorescence of the green channel disappeared while the red channel remained unchanged (Figure 6B). Next, we continued to pretreat HepG2 cells with Cys for 1h, then co-incubate with probe **LXB** (10 μM) for 30 min. The fluorescence in the green channel is significantly enhanced, while the red channel remains unchanged (Figure 6C). Finally, HepG2 cells were pretreated with Lipopolysaccharide (LPS, 10 μg/mL) for 6 h to induce endogenous production. After coincubation with probe **LXB** (10 μM) for 30 min, the fluorescence of the red and green channels disappeared (Figure 6D). These experimental results indicated that the probe can simultaneously detect changes of Cys and $ONOO^-$ in cells.

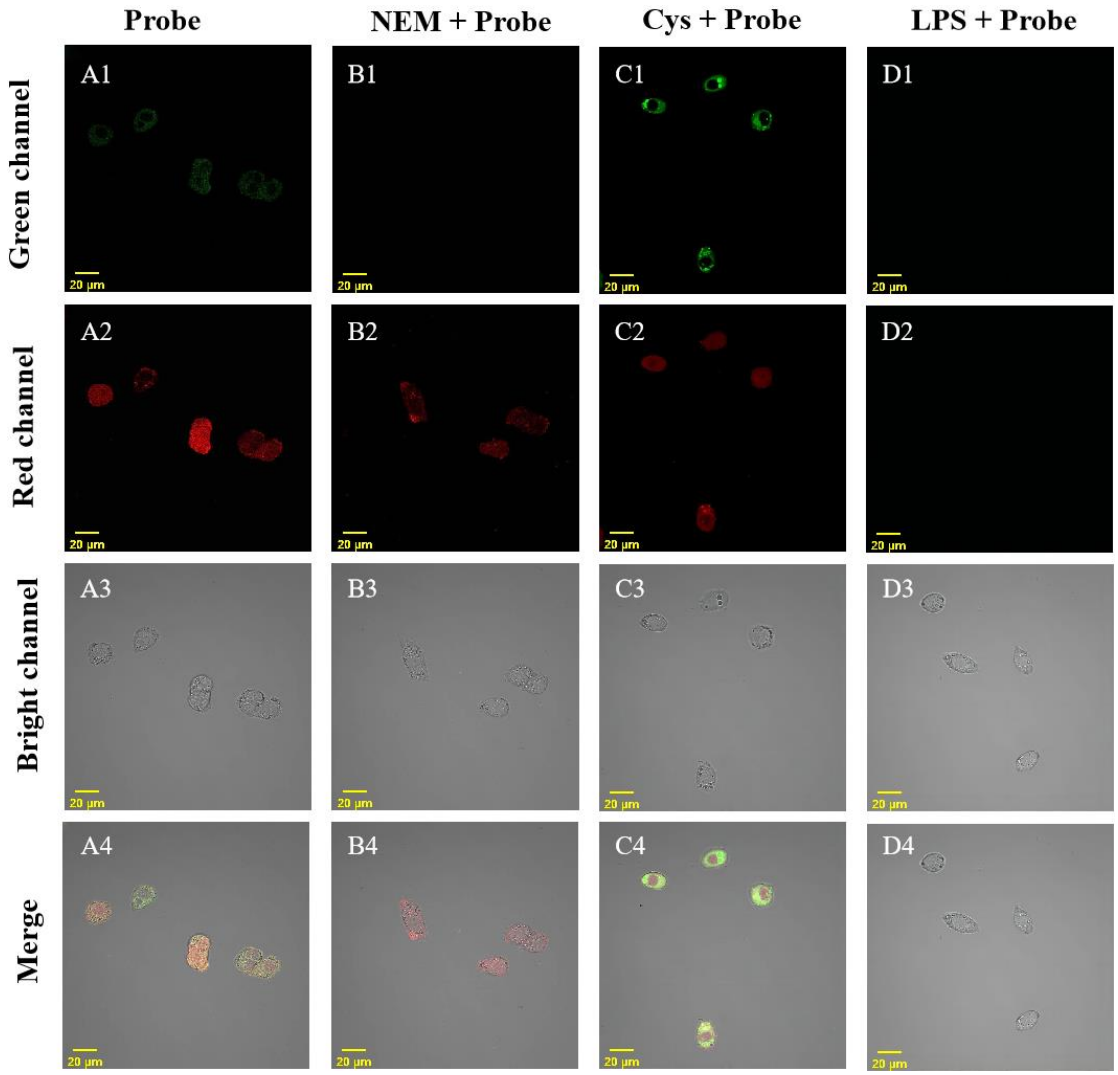

Figure 6. HepG2 cells were subjected to various treatments: (A1-A4) probe **LXB** 10 μM for 30 min; (B1-B4) 2 mM NEM for 1 h and then incubated with probe **LXB** 10 μM for 30 min; (C1-C4) 2 mM Cys for 1 h and then incubated with probe **LXB** 10 μM for 30 min; (D1-D4) LPS (10 μg / mL) for 8 h and then incubated with probe **LXB** 10 μM for 30 min. Green channel：λ_{em} = 460-500 nm (λ_{ex} = 405 nm). Red channel: λ_{em} = 560-660 nm (λ_{ex} = 488 nm). Scale bar : 20 μm.

3.7 Fluorescence imaging with ferroptosis

Erastin is a well-established drug known for its ability to induce cell ferroptosis. The intracellular ferroptosis can be achieved by targeting the system X_c^-. **LXB** (10 μM) was incubated with erastin (10 μM) and HepG2 cells separately for 0, 0.5, 1, 1.5, and 2 h, followed by imaging under a confocal microscope. The results shown in Figure 7 demonstrated that within the 0-2 h time frame, the fluorescence of the green channel

first decreased and then increased, while the fluorescence of the red channel decreased and then increased. These results mean that intracellular Cys first decreased and then increased, while the same $ONOO^-$ first increased and then decreased, and finally maintains a relatively low level. This may be due to the induction of oxidative stress by erastin. Similarly, we incubated HepG2 cells with probe **LXB** (10 μM), erastin (10 μM), and Fer-1(15 μM) respectively for 0 h, 0.5, 1, 1.5, and 2 h. Interestingly, no significant changes in intracellular fluorescence were observed (Figure 8). These findings provide evidence that erastin promotes ferroptosis and induces rapid cell death by blocking the transport function of the X_c^- cystine transporter, leading to a depletion of GSH.

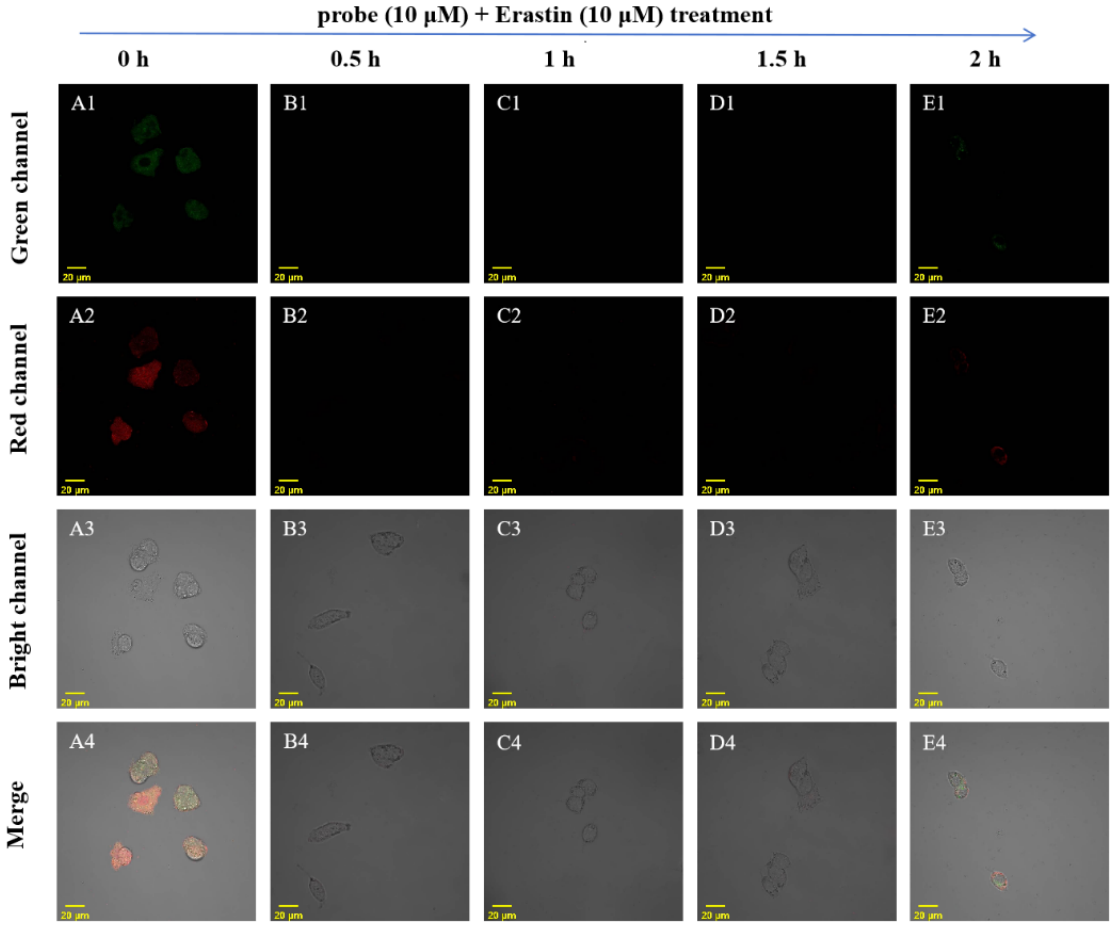

Figure 7. Fluorescence time images of HepG2 cells incubated with probe **LXB** (10 μM) and erastin (10 μM) (0-2 h). Green channel：λ_{em} = 460-500 nm (λ_{ex} = 405 nm). Red channel：λ_{em} = 560-660 nm (λ_{ex} = 488 nm). Scale bar: 20 μm.

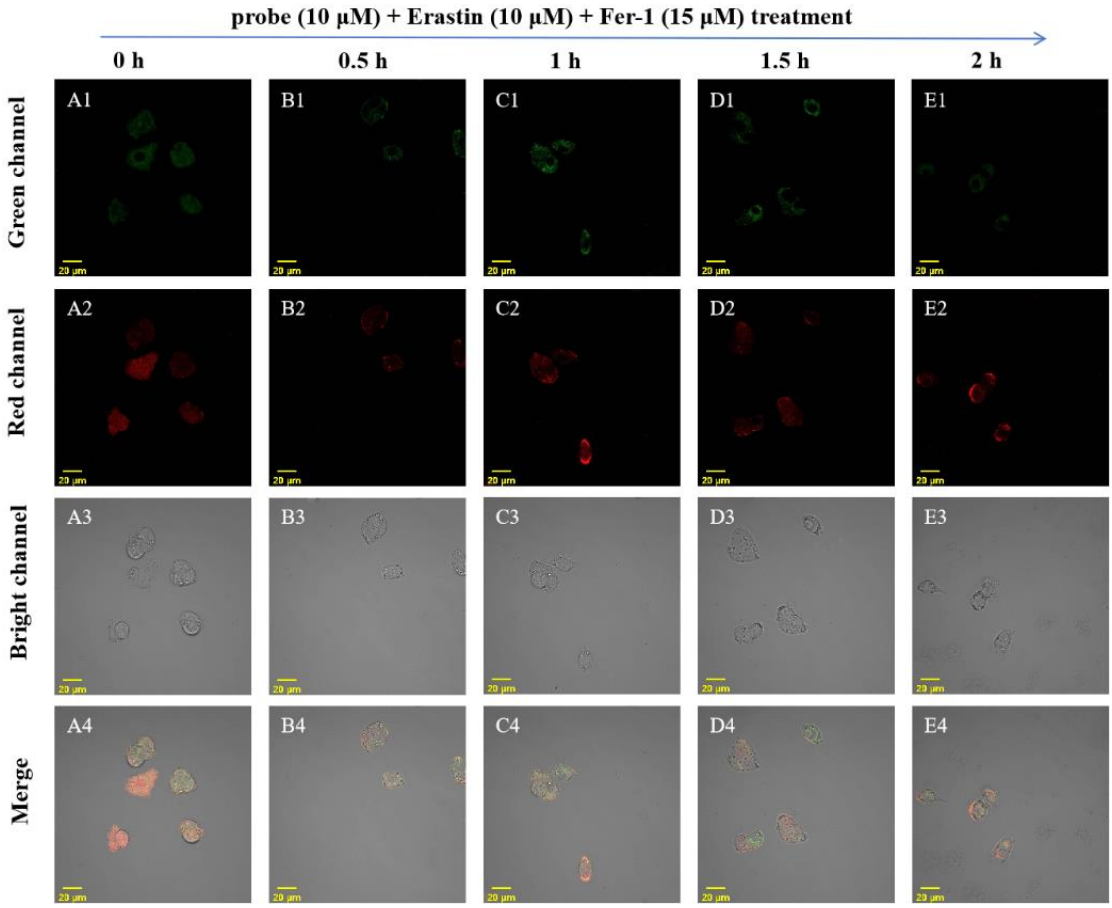

Figure 8. Fluorescence time images of HepG2 cells incubated with probe **LXB** (10 μM) and then treated with erastin (10 μM) and Fer-1(15 μM) (0-2 h). Green channel：λ_{em} = 460-500 nm (λ_{ex} = 405 nm). Red channel：λ_{em} = 560-660 nm (λ_{ex} = 488 nm). Scale bar: 20 μm.

4 Conclusion

In summary, we have designed a novel dual channel excited fluorescent probe **LXB** for detecting Cys and $ONOO^-$ through the green and red fluorescence channels, respectively (λ_{em} = 498 nm for Cys and λ_{em} = 565 nm for $ONOO^-$). The detection limits of probe **LXB** were 1.31 μM and 3.89 μM, respectively, and it is not affected by other ions. Furthermore, cell experiments have shown that the probe has lower toxicity and can detect exogenous Cys and endogenous $ONOO^-$. Moreover, cell ferroptosis experiments have demonstrated that the probe could monitor intracellular ferroptosis, provides a reliable method to further study the mechanism of ferroptosis and the treatment of cancer.

Author statement

Xiongbo Liu: Methodology, Data curation, Writing-Original Draft. Jiali Zhu: Validation. Qiangsheng Zhang: Validation. Hao Hu: Investigation. Wei Zhang: Investigation. Hui Xu: Investigation. Yan Huang: Investigation. Jialin Xie: Investigation. Hongtao Liu: Investigation. Yan Feng: Writing-Review & Editing, Visualization. Jianwei Li: Writing-Review & Editing, Visualization. Chunman Jia: Writing-Review & Editing, Visualization.

Conflicts of interest

There are no conflicts to declare.

Acknowledgments

We are grateful for the financial support from the National Natural Science Foundation of China (22161017, 22161016), the Start-up Research Foundation of Hainan University (KYQD(ZR) 23084, KYQD(ZR)22034) and Innovational Fund for Scientific and Technological Personnel of Hainan Province (KJRC2023D34).

Reference

[1] Scott J. Dixon, Kathryn M. Lemberg, Michael R. Lamprecht, R. Skouta, Eleina M. Zaitsev, Caroline E. Gleason, Darpan N. Patel, Andras J. Bauer, Alexandra M. Cantley, Wan S. Yang, B. Morrison, Brent R. Stockwell, Ferroptosis: an iron-dependent form of nonapoptotic cell death, Cell, 149 (2012) 1060-1072.

[2] B.R. Stockwell, J.P. Friedmann Angeli, H. Bayir, A.I. Bush, M. Conrad, S.J. Dixon, S. Fulda, S. Gascon, S.K. Hatzios, V.E. Kagan, K. Noel, X. Jiang, A. Linkermann, M.E. Murphy, M. Overholtzer, A. Oyagi, G.C. Pagnussat, J. Park, Q. Ran, C.S. Rosenfeld, K. Salnikow, D. Tang, F.M. Torti, S.V. Torti, S. Toyokuni, K.A. Woerpel, D.D. Zhang, Ferroptosis: a regulated cell death nexus linking metabolism, redox biology, and disease, Cell, 171 (2017) 273-285.

[3] Y. Lin, W. Xu, Y. Hou, S. Wang, H. Zhang, M. Ran, Y. Huang, Y. Wang, G. Yang, The multifaceted role of ferroptosis in kidney diseases, Chem. Biol. Interact, 365 (2022) 110107.

[4] W.S. Yang, R. SriRamaratnam, M.E. Welsch, K. Shimada, R. Skouta, V.S. Viswanathan, J.H. Cheah, P.A. Clemons, A.F. Shamji, C.B. Clish, L.M. Brown, A.W. Girotti, V.W. Cornish, S.L. Schreiber, B.R. Stockwell, Regulation of ferroptotic cancer cell death by GPX4, Cell, 156 (2014) 317-331.

[5] G. Powis, M. Briehl, J. Oblong, Redox signalling and the control of cell growth and death, Pharmacol. Therapeut, 68 (1995) 149-173.

[6] B.L. Dong, S.J. Li, Y. Wang, X.C. Tang, R.f. Wang, X.Q. Kong, T. Yue, Recent advance in the development of the fluorescent responsive probes for the study of ferroptosis, TrAC, Trends Anal. Chem., 168 (2023) 117327.

[7] S. Bartesaghi, R. Radi, Fundamentals on the biochemistry of peroxynitrite and protein tyrosine nitration, Redox Biol, 14 (2018) 618-625.

[8] H.R. Choi, J.S. Choi, Y.N. Han, S.J. Bae, H.Y. Chung, Peroxynitrite scavenging activity of herb extracts, Phytother. Res, 16 (2002) 364-367.

[9] G. Ferrer-Sueta, R. Radi, Chemical biology of peroxynitrite: kinetics, diffusion, and radicals, ACS Chem. Biol, 4 (2009) 161-177.

[10] P.H. Chan, Oxygen radicals in focal cerebral ischemia, Brain Pathol, 4 (1994) 59-65.

[11] Y. Sun, X. Tang, X. Li, X. Kong, M. Tian, Y. Wang, B. Dong, PET-ESIPT-based fluorescent probes for revealing the fluctuation of peroxynitrite ($ONOO^-$) in living cells, zebrafishes and brain tissues, Sensor. Actuat. B, 353 (2022) 131121.

[12] H. Jaeschke, C.D. Williams, A. Ramachandran, M.L. Bajt, Acetaminophen hepatotoxicity and repair: the role of sterile inflammation and innate immunity, Liver Int, 32 (2012) 8-20.

[13] V.I. Lushchak, Glutathione homeostasis and functions: potential targets for medical interventions, J. Amino Acids, 2012 (2012) 736837.

[14] S.M. Naushad, A. Radha Rama Devi, S. Nivetha, G. Lakshmitha, A.B. Stanley, T. Hussain, V.K. Kutala, Neuro-fuzzy model of homocysteine metabolism, Am. J. Hum. Genet, 96 (2017) 919-926.

[15] J.B. Schulz, J. Lindenau, J. Seyfried, J. Dichgans, Glutathione, oxidative stress and neurodegeneration, Eur. J. Biochem, 267 (2000) 4904-4911.

[16] Y.H. Sun, H.H. Han, J.M. Huang, J. Li, Y. Zang, C.Y. Wang, A long-wavelength fluorescent probe with a large Stokes shift for lysosome-targeted imaging of Cys and GSH, Spectrochim. Acta. Part A, 261 (2021) 120055.

[17] J. Lewerenz, S.J. Hewett, Y. Huang, M. Lambros, P.W. Gout, P.W. Kalivas, A. Massie, I. Smolders, A. Methner, M. Pergande, S.B. Smith, V. Ganapathy, P. Maher, The cystine/glutamate antiporter system xc− in health and disease: from molecular mechanisms to novel therapeutic opportunities, Antioxid. Redox

Signal, 18 (2013) 522-555.
[18] A. Pompella, A. Visvikis, A. Paolicchi, V.D. Tata, A.F. Casini, The changing faces of glutathione, a cellular protagonist, Adv. Biochem. Pharmacol, 66 (2003) 1499-1503.
[19] S. Lanzardo, L. Conti, R. Rooke, R. Ruiu, N. Accart, E. Bolli, M. Arigoni, M. Macagno, G. Barrera, S. Pizzimenti, L. Aurisicchio, R.A. Calogero, F. Cavallo, Immunotargeting of antigen xCT attenuates stem-like cell behavior and metastatic progression in breast cancer, Acad. J. Cancer Res, 76 (2016) 62-72.
[20] M. Conrad, H. Sato, The oxidative stress-inducible cystine/glutamate antiporter, system xc−: cystine supplier and beyond, J. Amino Acids, 42 (2012) 231-246.
[21] B. Niu, K. Liao, Y. Zhou, T. Wen, G. Quan, X. Pan, C. Wu, Application of glutathione depletion in cancer therapy: enhanced ROS-based therapy, ferroptosis, and chemotherapy, Biomaterials, 277 (2021) 121110.
[22] Z. Li, Y. Li, Y. Yang, Z. Gong, H. Zhu, Y. Qian, In vivo tracking cystine/glutamate antiporter-mediated cysteine/cystine pool under ferroptosis, Anal. Chim. Acta, 1125 (2020) 66-75.
[23] S. Galadari, A. Rahman, S. Pallichankandy, F. Thayyullathil, Reactive oxygen species and cancer paradox: To promote or to suppress?, Free Radical Biol. Med, 104 (2017) 144-164.
[24] C.E. Paulsen, K.S. Carroll, Cysteine-mediated redox signaling: chemistry, biology, and tools for discovery, Chem. Rev, 113 (2013) 4633-4679.
[25] B. Zhou, B. Wang, M. Bai, M. Dong, X. Tang, Fluorescent probe for highly selective detection of cysteine in living cells, Spectrochim. Acta. Part A, 294 (2023) 122523.
[26] Wan S. Yang, R. SriRamaratnam, Matthew E. Welsch, K. Shimada, R. Skouta, Vasanthi S. Viswanathan, Jaime H. Cheah, Paul A. Clemons, Alykhan F. Shamji, Clary B. Clish, Lewis M. Brown, Albert W. Girotti, Virginia W. Cornish, Stuart L. Schreiber, Brent R. Stockwell, Regulation of ferroptotic cancer cell death by GPX4, Cell, 156 (2014) 317-331.
[27] R.V. Swanda, Q. Ji, X. Wu, J. Yan, L. Dong, Y. Mao, S. Uematsu, Y. Dong, S.-B. Qian, Lysosomal cystine governs ferroptosis sensitivity in cancer via cysteine stress response, Molecular Cell, 83 (2023) 3347-3359.e3349.
[28] W. Yang, R. Liu, X. Yin, Y. Jin, L. Wang, M. Dong, K. Wu, Z. Yan, G. Fan, Z. Tang, Y. Li, H. Jiang, Peroxynitrite activated near-infrared fluorescent probe for evaluating ferroptosis-mediated acute kidney injury, Sensor. Actuat. B, 393 (2023) 134180.
[29] H. Yan, X. Xu, J. Li, P. Xie, W. Cao, X. Yang, Y. Ye, A novel fluorescence-on fluorescent probe for $ONOO^-$ detection in HeLa cells, J. Photoch. Photobio. A, 440 (2023) 114638.
[30] F. Zhang, X. Liang, W. Zhang, Y. L. Wang, H. Wang, Y.H. Mohammed, B. Song, R. Zhang, J. Yuan, A unique iridium(III) complex-based chemosensor for multi-signal detection and multi-channel imaging of hypochlorous acid in liver injury, Biosens. Bioelectron, 87 (2017) 1005-1011.
[31] W. Qu, C. Niu, X. Zhang, W. Chen, F. Yu, H. Liu, X. Zhang, S. Wang, Construction of a novel far-red fluorescence light-up probe for visualizing intracellular peroxynitrite, Talanta, 197 (2019) 431-435.
[32] H.W. Liu, L. Chen, C. Xu, Z. Li, H. Zhang, X. B. Zhang, W. Tan, Recent progresses in small-molecule enzymatic fluorescent probes for cancer imaging, Chem. Soc. Rev, 47 (2018) 7140-7180.
[33] X. Jia, Q. Chen, Y. Yang, Y. Tang, R. Wang, Y. Xu, W. Zhu, X. Qian, FRET-based mito-specific fluorescent probe for ratiometric detection and imaging of endogenous peroxynitrite: dyad of Cy3 and Cy5, J. Am. Chem. Soc, 138 (2016) 10778-10781.
[34] Z. Zhan, R. Liu, L. Chai, Y. Dai, Y. Lv, Visualization of lung inflammation to pulmonary fibrosis via peroxynitrite fluctuation, Anal. Chem, 91 (2019) 11461-11466.

[35] B. Tang, Y. Xing, P. Li, N. Zhang, F. Yu, G. Yang, A rhodamine-based fluorescent probe containing a Se−N bond for detecting thiols and its application in living cells, J. Am. Chem. Soc, 129 (2007) 11666-11667.

[36] X. Chen, Y. Zhou, X. Peng, J. Yoon, Fluorescent and colorimetric probes for detection of thiols, Chem. Soc. Rev, 39 (2010) 2120-2135.

[37] Z. Mao, J. Xiong, P. Wang, J. An, F. Zhang, Z. Liu, J. Seung Kim, Activity-based fluorescence probes for pathophysiological peroxynitrite fluxes, Coordin. Chem. Rev, 454 (2022) 214356.

[38] Y. Ji, S. Liu, J. Zhang, L. Qu, J. Wu, H. Liu, Z. Cheng, Construction of HPQ-based activatable fluorescent probe for peroxynitrite and its application in ferroptosis and mice model of LPS-induced inflammation, Bioorg. Chem, 138 (2023) 106650.

[39] L. Ma, Q. Yang, Q. Zan, H. Tian, X. Zhang, C. Dong, L. Fan, A benzothiazole-based fluorescence probe for imaging of peroxynitrite during ferroptosis and diagnosis of tumor tissues, Anal. Bioanal. Chem, 414 (2022) 7753-7762.

[40] F. Xie, R. Zhou, C. Jian, L. Zhang, Y. He, A borate-based peroxynitrite fluorescent probe and its application in fluorescence imaging of living cells, Anal. Methods, 15 (2023) 3268-3274.

[41] H. Zhao, Y. Xiong, L. Zang, J. Lu, Radical nucleophilic substitution/cyclization: A novel strategy for selective and ultrafast fluorescence imaging of cysteine levels in ferroptosis process, Talanta, 253 (2023) 123917.

[42] Y. Chen, Z. Hu, M. Yang, J. Gao, J. Luo, H. Li, Z. Yuan, Monitoring the different changing behaviors of •OH and cysteine in two ferroptosis pathways by a dual-functional fluorescence probe, Sensor. Actuat. B, 362 (2022) 131742.

[43] L.L. Wang, Y.R. Zhang, M.H. Zheng, X. Wang, X. Wu, J.Y. Jin, A single fluorescent probe reveals changes in endoplasmic reticulum–mitochondria contact in hepatocytes during ferroptosis, Chem. Eng. J, 466 (2023) 143104.

[44] Y. Wang, H. Yan, Y. Yue, Y. Zhang, F. Huo, F. Cheng, C. Yin, GSH and H_2O_2 dynamic correlation in the ferroptosis pathways revealed by engineered probe in tumor and kidney injury, Chem. Eng. J, 464 (2023) 142496.

[45] I. Yahaya, N. Seferoğlu, Z. Seferoğlu, Improved one-pot synthetic conditions for synthesis of functionalized fluorescent coumarin-thiophene hybrids: syntheses, DFT studies, photophysical and thermal properties, Tetrahedron, 75 (2019) 2143-2154.

[46] Himangini, D.P. Pathak, V. Sharma, S. Kumar, Designing novel inhibitors against falcipain-2 of Plasmodium falciparum, Bioorg. Med. Chem. Lett, 28 (2018) 1566-1569.

[47] T. Lu, F. Chen, Multiwfn: a multifunctional wavefunction analyzer, J. Comput. Chem, 33 (2012) 580-592.

[48] Y. Sun, R. Wang, J. Wang, H. Wei, Q. Chen, Y. Wang, B. Dong, Construction of a ratiometric two-photon ER-targeting fluorescent probe for the imaging of peroxynitrite in living systems, Sensor. Actuat. B, 370 (2022) 132439.

[49] A.M.A. Abdulkhaleq, Y. Zhao, K. Qian, X. Wang, Z. Zuo, X. Zhou, Development of highly selective novel fluorescence turn-on probe based on carbon dots for sensing peroxynitrite ($ONOO^-$) in vitro and in vivo, Dyes Pigm, 217 (2023) 111404.

[50] M. Li, H. Han, H. Zhang, S. Song, S. Shuang, C. Dong, Boronate based sensitive fluorescent probe for the detection of endogenous peroxynitrite in living cells, Spectrochim. Acta. Part A, 243 (2020) 118683.